Prepared for submission to JINST

Characterization of FBK SiPM sensors for the DUNE Far detector 1 Photon Detection System

F. Acerbi[0] M. Andreotti,[2] A. Balboni,[2,3] E. Bertolini,[4,5] S. Bertolucci,[6,7] F. Bramati,[4,5] A. Branca,[5,6] C. Brizzolari,[5,5] G. Brunetti,[4,5] R. Calabrese,[2,3] E. Calvo,[8] P. Carniti,[4,5] D. Casazza,[2,3] C. Cattadori,[4] A. Cervera,[9] S. Chiozzi,[2] V. Cicero,[6] A. Cotta Ramusino,[2] E. Cristaldo Morales,[4,5] C. Cuesta,[8] R. D'Amico,[2,3] M. Delgado Gonzalez,[4,5] F. Di Capua,[10,11] D. Di Ferdinando,[6] A. Dyshkant,[12] M. Eads,[12] A. Falcone,[4,5] E. Fialova,[13] A. Ficorella[1] M. Fiorini,[2,3] K. Francis,[12] A. Gabrielli,[6,7] F. Galizzi,[4,5] G. Gallina,[14,15] D. Garcia-Gamez,[16] M. Á. García-Peris,[9] T. Giammaria,[2,3] I. Gil-Botella,[8] A. Gola[1] C. Gotti,[4] M. Guarise,[2,3] D. Guffanti,[4,5] I. Lax,[6] I. López de Rego,[8] E. Luppi,[2,3] S. Manthey,[8] J. Martin-Albo,[9] N. Mauri,[6,7] L. Meazza,[4,5] A. Minotti,[4,5] E. Montagna,[6,7] A. Montanari,[6,7] I. Neri,[2,3] F. J. Nicolas-Arnaldos,[16] C. Palomares,[8] L. Parellara Monreal[1] L. Pasqualini,[6,7] G. Paternoseter[1] L. Pérez-Molina,[8] G. Pessina,[4] V. Pia,[6] L. Pierini,[2,3] F. Poppi,[6] M. Pozzato,[6] M. Querol,[9] F. Retiere,[15] J. Rocabado,[9] A. Saadana,[9] A. Sanchez-Castillo,[16] P. Sanchez-Lucas,[16] A. Scanu,[4,5] F. S. Schifano,[2,3] G. Sirri,[6] J. Smolik,[13] M. Tenti,[6] F. Terranova,[4,5] L. Tomassetti,[2,3] M. Torti,[4,5] N. Tosi,[6] A. Verdugo de Osa,[8] H. Vieira de Souza,[17] J. Zalesak,[18] B. Zamorano,[16] S. Zucchelli,[6,7] V. Zutshi.[12]

[1]*Fondazione Bruno Kessler, 38123 Trento, Italy*
[2]*Istituto Nazionale di Fisica Nucleare, Sezione di Ferrara, I-44122 Ferrara, Italy*
[3]*Università degli Studi di Ferrara, 44122 Ferrara, Italy*
[4]*Istituto Nazionale di Fisica Nucleare Sezione Milano Bicocca*
[5]*Università di Milano Bicocca, Dipartimento di Fisica*
[6]*Istituto Nazionale di Fisica Nucleare Sezione di Bologna, 40127 Bologna, Italy*
[7]*Università di Bologna, 40127 Bologna, Italy*
[8]*CIEMAT, Centro de Investigaciones Energéticas, Medioambientales y Tecnológicas, E-28040 Madrid,*
[9]*Instituto de Física Corpuscular, Valencia, Spain*
[10]*Istituto Nazionale di Fisica Nucleare Sezione di Napoli, Naples, Italy*
[11]*Università degli Studi di Napoli Federico II*
[12]*Northern Illinois University, Department of Physics*
[13]*Czech Technical University, 115 19 Prague 1, Czech Republic*
[14]*Physics Department, Princeton University, Princeton, NJ 08544, USA*
[15]*TRIUMF, 4004 Wesbrook Mall, Vancouver, BC V6T 2A3, Canada*
[16]*University of Granada & CAFPE, Campus Fuentenueva (Edif. Mecenas), 18002 Granada, Spain*
[17]*APC, Laboratoire Astroparticule et Cosmologie, Université de Paris Cité, Paris, France*
[18]*Institute of Physics, Czech Academy of Sciences, 182 00 Prague 8, Czech Republic*

Abstract: The Deep Underground Neutrino Experiment (DUNE) is a long baseline neutrino experiment based in the USA and composed of a Near Detector (ND) complex at FermiLab and a Far Detector (FD) complex located at the SURF Underground Laboratory ~1300 km distant. DUNE will study the neutrino oscillations looking for CP violation in leptonic sector starting from the early 2030s. The FD modules will be composed of four Liquid Argon Time Projection Chambers (LAr TPC) each one with a volume of 17kton that will exploit both charge and light signals to detect neutrino interactions with Argon. The light signals produced by the scintillating photons in LAr will be detected by the Photon Detection System (PDS) based on light collectors coupled to Silicon Photomultipliers (SiPMs). During a test campaign, different laboratories of the collaboration performed an investigation of the best SiPM candidates that fulfill the DUNE FD requests. We identified two models of SiPM, produced by Hamamatsu Photonics K.K. (HPK) and Fondazione Bruno Kessler (FBK), respectively. In this paper, we focus on the FBK selected model showing its main features. We will describe the characterization protocol, the results at room and cryogenic temperatures and the photon detection efficiency measurements.

Keywords: Photon detectors for UV, visible and IR photons (solid-state), Photon detectors for UV, visible and IR photons (solid-state) (PIN diodes, APDs, Si-PMTs, G-APDs, CCDs, EBCCDs, EMCCDs, CMOS imagers, etc), Time projection Chambers, Neutrino detectors

Contents

1 Introduction

DUNE (Deep Underground Neutrino Experiment) is a next-generation long baseline neutrino experiment whose main goal will be a detailed study of neutrino oscillation. DUNE will consist of a NEAR detector (ND) placed in proximity of the neutrino production site at Fermi National Laboratory, and of a FAR detector (FD) that will be installed in the Surf Underground Laboratory in South Dakota [1]. The DUNE Far Detector module one (FD1) will be a liquid argon time projection chamber (LAr TPC) with an Horizontal Drift (HD) configuration and a total mass of nearly 70 kt. Beyond charge signals, DUNE FD1-HD will also exploit the scintillation light of argon whose peak wavelength is 127 nm [2]. Light signals will be collected in the Photon Detection System (PDS) thanks to the so-called X-ARAPUCA modules. These modules allows to trap photons inside a highly reflective box that contains wavelength shifting bars and visible sensitive Silicon Photo-Multipliers (SiPM) sensors [3].

FD1-HD will employ SiPMs produced by two different companies: Fondazione Bruno Kessler (FBK) and Hamamatsu Photonics K.K (HPK) [4]. Both models are designed for the use at cryogenic temperatures and have an effective area of around 36 mm^2, while they have different characteristics in terms of the cell pitch, the breakdown voltage and the quenching resistor. These models have been selected after an R&D phase, carried out by the PDS Consortium, in collaboration with the manufacturers, looking for the prototypes that addressed the technical requirements for the FD1-HD. The tests concerning FBK CRYO-NUV-HD-3T sensors, that will be presented in this paper, have been performed in seven different test sites of the PDS Consortium: Bologna (*Istituto*

Nazionale di Fisica Nucleare and *Università di Bologna*), DeKalb (*Northern Illinois University, Department of Physics*), Ferrara (*Istituto Nazionale di Fisica Nucleare* and *Università di Ferrara*), Madrid (*CIEMAT, Centro de Investigaciones Energéticas, Medioambientales y Tecnológicas*), Milano (*Istituto Nazionale di Fisica Nucleare* and *Università di Milano-Bicocca*), Prague (*Institute of Physics, Czech Academy of Sciences*), and Valencia (*Instituto de Física Corpuscular*).

The paper is organized as follows: in the first section 2.3 a detailed description of the main features of the FBK sensors customized for DUNE compared to the other FBK models. In the second section 3 there is a description of the measurements performed by the PDS consortium members to characterize the SiPMs at cryogenic temperatures with a adescription of the setup and procedure used. Then, a dedicated section 4 describes the Photo Detection Efficiency (PDE) measurements. Eventually, there will be the discussions of the results and the conclusions.

2 SiPM features

2.1 NUV-HD-Cryo Technology

Over the years, FBK has developed various technologies of SiPMs to obtain optimal performances to meet the requirements of different experiments and applications. Silicon Photomultipliers are matrices of Single-photon avalanche diodes (SPADs) each one with an integrated quenching resistor and connected together in parallel forming a single sensor. Depending on the type of epitaxial layer used for the fabrication, we can distinguish two families of technologies: p-on-n junction with an n-type epitaxial layer labeled as FBK NUV-HD technologies characterized by a peak detection efficiency in the near-UV[5], and n-on-p junction with a p-type epitaxial layer named FBK RGB/NIR-HD, featuring a peak detection efficiency at longer wavelengths[6][7]. Starting from the standard NUV-HD technology, a customization of the electric field was implemented to develop the NUV-HD-Cryo SiPM technology for cryogenic applications such as in the DarkSide experiment. Strengths of this technology are a very low dark count rate in the order of few mHz/mm^2 at cryogenic temperature and a lower afterpulsing probability, as a result of a low peak value of the electric field compared to the standard FBK technology[8].

2.2 DUNE Customization

In the framework of the DUNE experiment, a dedicated customization of the NUV-HD-Cryo SiPM technology was carried out to improve the performance of the detectors to better comply with the experiment requirements. The gain of a SiPM microcell, defined as the number of carriers generated during an avalanche process, is a key factor to improve the signal to noise ratio enhancing the output signal. During the avalanche build-up the number of generated carriers is proportional to the active area of the microcell, thus increasing the cell size the gain increases. However, this gain increment comes with a drawback of a higher correlated noise (optical crosstalk), because the generation of secondary photons is proportional to the amount of carrier flowing during the avalanche. The aim of the DUNE customization was to modify the standard SiPM structure to obtain a device that combines a high gain and a limited crosstalk. This has been done by increasing the number of Deep Trench Isolation (DTI) between neighboring cells. Two different layout splits were produced and tested to evaluate the best option for the DUNE experiment, a $30\mu m$ cell pitch device with a standard single DTI to be used as a reference, and a $54\mu m$ cell pitch device with three DTIs.

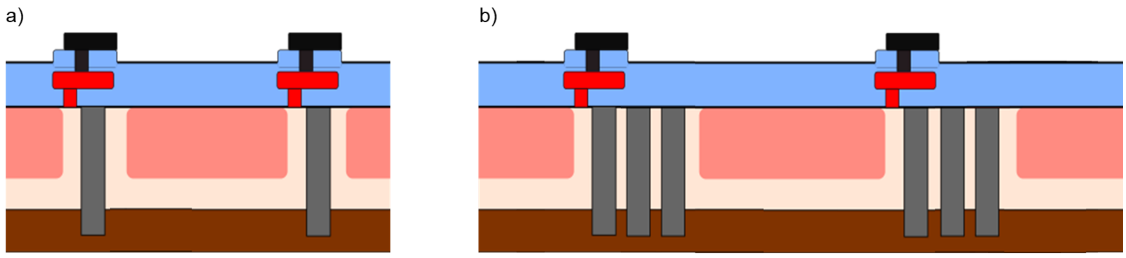

Figure 1. a) Cross-section of the 30μm cell pitch device with a standard single DTI (1T – 30μm), b) Cross-section of the 54μm cell pitch device with three DTIs (3T – 54μm).

In figure1 the cross-sections of the two different layout splits with all the basic features of the cell structure are depicted. The high-field region (pink structures in the figure) where the avalanche takes place is implemented by a high energy ion implantation. The quenching resistors, which are needed to quench and subsequently recharge the microcells, are represented in red, while the metal contacts are shown in black. On the top part of the cell, a passivation layer is represented in light blue. Each cell of the SiPM is separated by deep trenches (gray structures) filled with silicon dioxide that are effective to electrically isolate the cells and also partially optically isolate nearby cells from the crosstalk photons.

2.3 Features at room temperature

In this section the results of a functional characterization of the two layout splits are reported providing a comparison in terms of gain, crosstalk and PDE. The measurements were acquired placing the devices in a climatic chamber at 20 degrees Celsius following a procedure described in a dedicated paper[9]. The PDE was measured at room temperature by using a pulsed mode technique with a setup featuring an integration sphere and LEDs of different wavelength, for further details refers to [10].

In figure 2 the gain as a function of the overvoltage is shown. The gain of the triple trench is approximately 2.6 times the gain of the single trench split.

In figure 3 the direct crosstalk probability as a function of the overvoltage is reported. The single trench layout exhibits a slightly higher value with respect to the triple trench. Measurements were performed on test structures of 1x1mm^2 active area without any protection resin on top of the devices.

The PDE at 435 nm as a function of the overvoltage is shown in figure 4. Measurements were performed on a test structure of 1x1mm^2 active area with an epoxy resin layer of approximately 500 μm on top of the devices to to smooth the oscillations in the PDE spectrum created by the constructive and destructive interferences caused by the top ARC on SiPM area. PDE increases with increasing overvoltage thanks to the increased triggering probability, reaching a saturation level at higher overvoltage. The two different splits exhibit similar values as expected from the similar geometrical fill factor between the two layouts (75% and 77%).

As reported in this section, the two different layout splits exhibit similar Optical Crosstalk and PDE while the gain of the triple trench is 2.6 times the gain of the single trench split. The 54μmcell

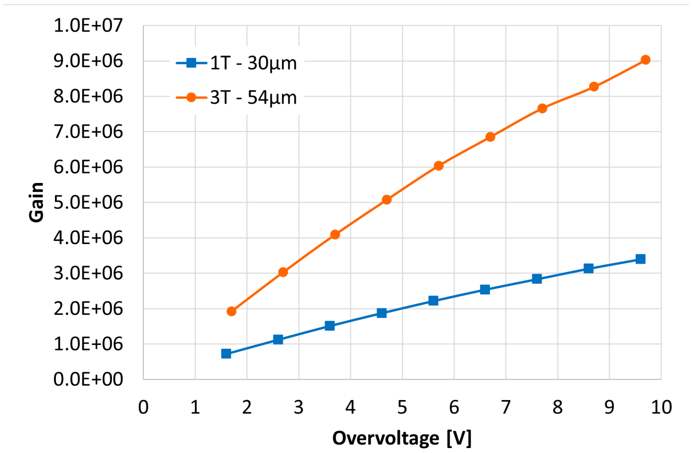

Figure 2. Comparison of the Gain as a function of the overvoltage between the two different splits (1T – 30μm; 3T – 54μm).

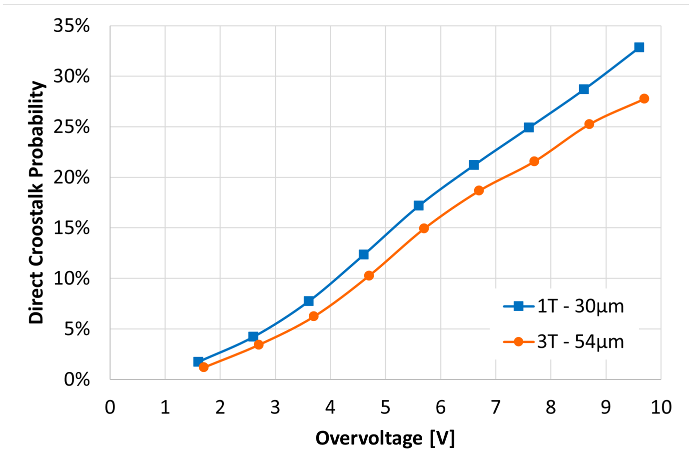

Figure 3. Comparison of the direct crosstalk probability as a function of the overvoltage between the two different splits (1T – 30μm; 3T – 54μm).

pitch device with three DTIs was selected for the DUNE experiment for its higher gain.

3 Cryogenic characterization

3.1 Experimental apparatus and procedure

Different institutions belonging to the PDS consortium of the DUNE collaboration were involved in the characterization of the sensors. These are: INFN and University of Bologna, INFN and University of Ferrara, CIEMAT Madrid, INFN and University of Milano Bicocca, INFN and University of Napoli, FZU Prague and IFIC Valencia. In addition, researchers from INFN and University of Napoli performed a dedicated measurement of the SiPM Photodetection Efficiency at liquid argon temperature, through a specific setup which will be described in section 4.

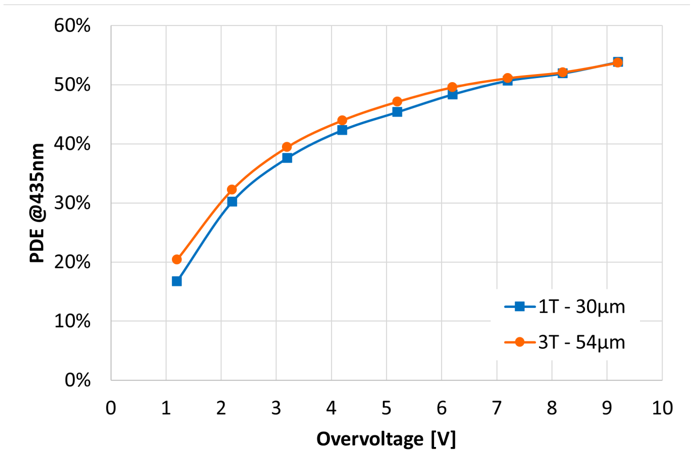

Figure 4. Comparison of the Photon Detection Efficiency (PDE) at 435nm as a function of the overvoltage between the two different splits (1T – 30μm; 3T – 54μm).

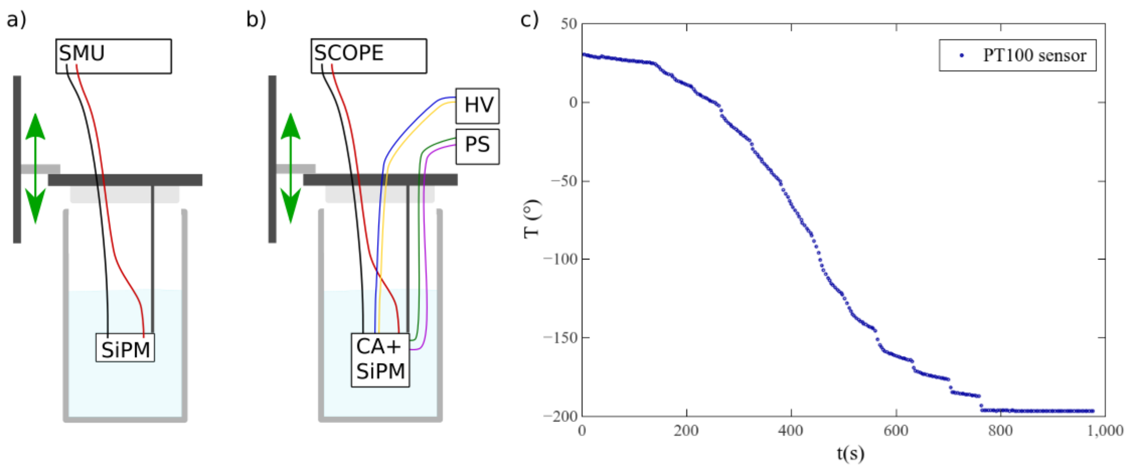

Figure 5. Setup used for the characterization of the sensors. a) Sketch of the apparatus used for IV measurements. b) Sketch of the apparatus used for DCR study, c) Temperature of the sensor during the diving in LN2 phase.

In order to guarantee compatible results in all the laboratories, each apparatus used for the tests complies with common specifications decided by the photon detection system consortium of DUNE. A detailed description of the prototype of the setup and the protocol followed during the measurements are provided in this section. Each laboratory have chosen similar solutions with same or best specifications.

The core of the setup consists of a liquid nitrogen dewar where the sensors are placed in order to perform tests at cryogenic temperatures. Depending on the type of measurements to perform, different commercial instruments, with different features, have been used. A picture that shows a sketch of the apparatus is shown in figure 5. The apparatus is also instrumented with a mechanical linear stage that allows to dive the sensors in liquid nitrogen following a controlled thermal profile.

This can be done thanks to a temperature sensor placed in the proximity of the SiPM. An example of a typical thermal profile during the diving phase is shown in figure 5-c.

The SiPMs IV measurements have been performed by a commercial source meter unit (SMU) directly connected to the SiPM through triaxial cables while the Dark count rate (DCR) characterization required a more complex apparatus that exploit the SMU to bias the SiPM with a stabilized voltage, a cryogenic amplification stage and an oscilloscope to acquire the signals. For the IV measurements, the minimum requirements for the SMU are (0-60) V voltage range, 10 pA precision, 6 digit resolution used with cables whose loss is less than 10 pA.

For the dark noise and gain measurements, the amplification stage is common for all the labs and is described in a dedicated paper [11]. The output of the amplifier is connected to the input of a digital oscilloscope, whose minimum requirements, established by the PDS consortium, are 1 GHz bandwidth, 5 Gs/s and 8 bit resolution. The DCR measurement is performed in a completely dark environment at three different values of over voltage V_{OV}, acquiring the waveforms with a trigger threshold of 0.5 photoelectron. We perform a dedicated analysis based on single signals observing their temporal and amplitude distributions.

The measurements sequence has also been defined to be common to all the labs involved in the test characterization. It has been organized as follows:

- IV curve at room temperature;
- 1^{st} diving phase;
- IV curve at LN2 during the first thermal cycle;
- 18 thermal cycles;
- IV curve at LN2 at the 19^{th} thermal cycle;
- DCR at three different values of V_{OV} during the 20^{th} thermal cycle.

All the results are then compared and organized together to obtain common results that will be presented in this paper in section 3.2.

3.2 Cryogenic characterization results

With the setup described in section 3.1, the different laboratories performed an investigation of the main features of the FBK-TT SiPMs. We initially measured the current-voltage (IV) curve at room temperature and at LN2 both at the first immersion and after 19 thermal cycles. The IV curve allowed us to obtain the breakdown voltage (V_{BD}) and the quenching resistor (R_{q}). The breakdown voltage V_{BD} has been estimated looking at the peak of the normalized derivative of the IV curve in the reverse region, as decided within the PDS consortium. The maximum of the curve $I^{-1}dI/dV$ has been fitted with a polynomial function of 2^{nd} degree in order to estimate the best value of V_{BD}. In the forward region of the IV curve, a linear fit in the range [1.2-1.5] V allowed us to assign the value of the global quenching resistor of the sensor as the reciprocal of the angular coefficient. The value of the quenching resistor of each cell (R_{q}) can be then easily derived assuming equal resistors for each cell. In figure 6 are shown two examples of the measured IV and the fits in the forward and reverse regions while SiPM is kept at room temperature.

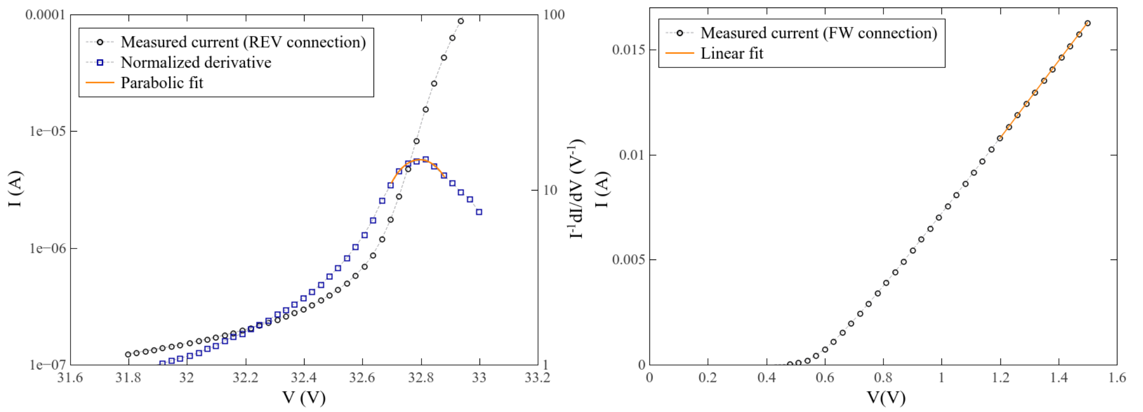

Figure 6. Left side: IV curve in reverse mode (REV). The normalized derivative and the parabolic fit are also shown in the plot. Right side: IV curve in the forward (FW) region.

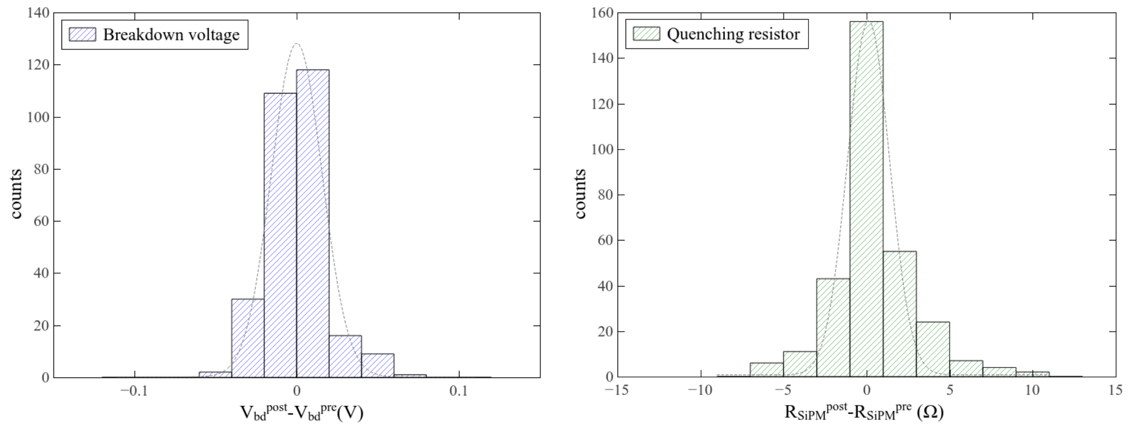

Figure 7. On the left part: histogram of the differences in the breakdown voltage values measured before and after the thermal cycles with a Gaussian distribution superimposed. On the right figure: histogram of the differences in the quenching resistor values measured before and after the thermal cycles with a Gaussian distribution superimposed.

In the table1 are summarized the main parameters obtained during IV measurements at room temperature and at LN2 after the 19^{th} thermal cycle.

Temperature	V_{bd} **(V)**	$R_q(k\Omega)$
300 K	33.0±0.1	**560**±10
77 K	27.08±0.03	2640±70

Table 1. Mean values for breakdown voltage and quenching resistor obtained from the various laboratories both at room temperature and at liquid nitrogen temperature.

In order to check the resilience of the sensors to the thermal stresses, we decided to check sensor by sensor the variation of both breakdown voltage and quenching resistor before and after

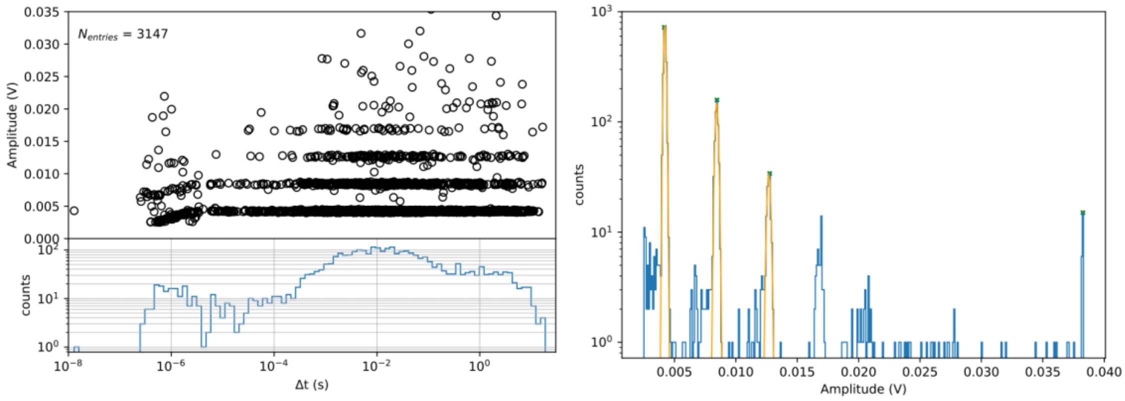

Figure 8. On the left part an example of a scatter plot of amplitude VS time delay between consecutive events (top) and the corresponding x-axis projection histogram (bottom). In the right part of the figure the amplitude histogram of single signals in logaritmic-scale is shown, it corresponds to the y-axis projection of the figure on the left. Yellow curves superimposed to the distribution represent the Gaussian fits of the 1p.e., 2p.e. and 3p.e. peaks.

the thermal cycle. Figure 7 shows on the left the histogram for the breakdown voltage difference where $V_{\mathrm{BD}}^{\mathrm{pre}}$ and $V_{\mathrm{BD}}^{\mathrm{post}}$ represent respectively the value at the 1^{st} and at the 19^{th} thermal cycle. The distribution is centered at 0 V as expected if no damages occur, and has a width calculated as the standard deviation of the Gaussian distribution of (31±2) mV. On the right part instead is shown the histogram of the resistors difference of the entire SiPMs (as calculated from the direct IV curve) measured after the thermal stresses ($R_{\mathrm{SiPM}}^{\mathrm{post}}$) and the one measured before ($R_{\mathrm{SiPM}}^{\mathrm{pre}}$). Also this last distribution is centered at 0 Ω and it has a standard deviation of (2.5 ± 0.1) Ω which is negligible, considering that the systematic uncertainty in the measurements of the resistor due to the electrical contacts at room and LN2 temperature can be estimated as few Ohms.

No values distant more than 70 mV and 10 Ω in the absolute value of the breakdown and quenching resistor respectively, have been found, indicating a good reproducibility of the measurements and no substantial variations in the SiPM main characteristics after thermal stresses.

After IV characterization each test site studied the behaviour of the SiPM in a completely dark environment at liquid nitrogen temperature. Thanks to the apparatus described in section 3.1, the acquired waveforms have been used to determine the temporal happening of single events and their amplitude. A typical example of 2-dim plot amplitude VS time delay, with all the components of the correlated noise, is shown in figure 8 on the left side. As clearly visible from the temporal distribution of the events, these SiPMs are affected by the so called burst effect, for which trains of consecutive pulses at kHz-rate happened. This phenomenon is better described in a dedicated paper [12] and is even present in the HPK lot of DUNE SiPMs [4]. On the right part of the figure the amplitude distribution of the events is shown .

Figure 9 summarizes the main results we obtained for the gain and the correlated noise characterization. The results are in accordance with the values provided by the vendor. The gain spans from $\sim 4.5 \cdot 10^6$ to $\sim 9 \cdot 10^6$ in the range [3.5-7] V of overvoltage which is within DUNE

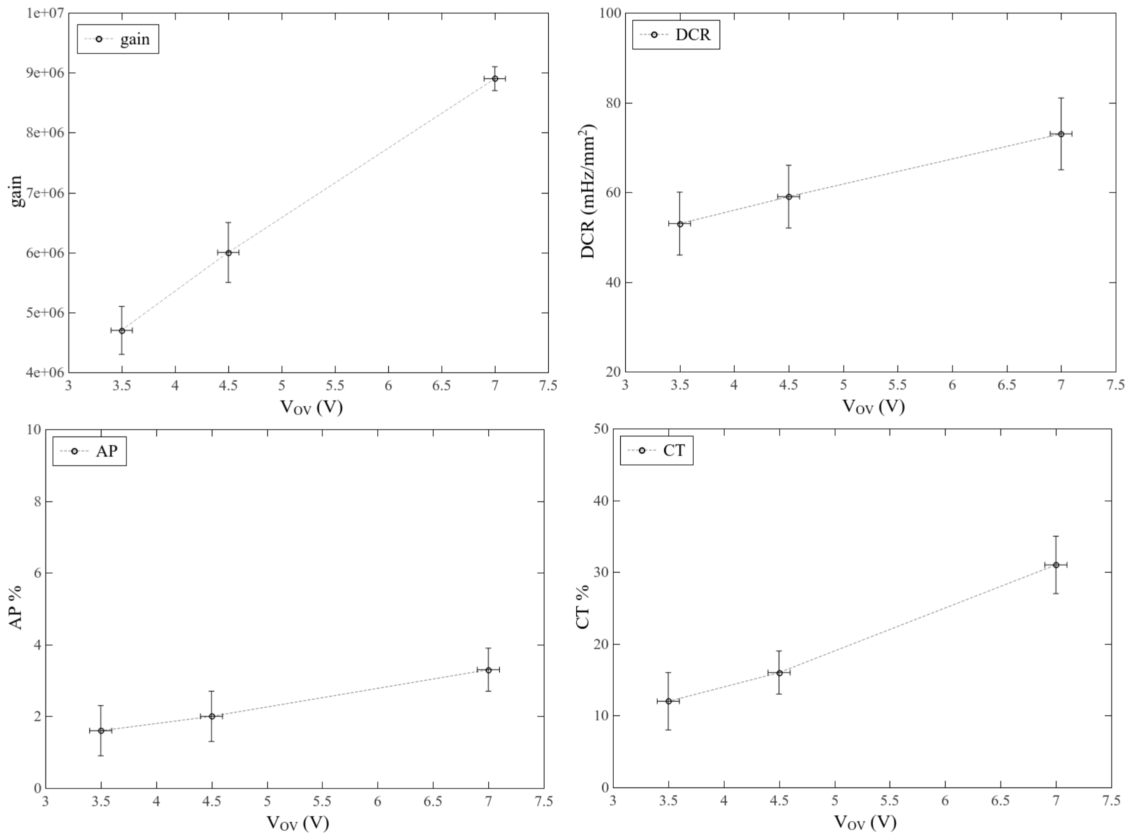

Figure 9. Results of the carachterization of the SiPMs. a) Gain as a function of the overvoltage. b) Dark count rate as a function of the overvoltage. c) Afterpulse and d) Direct plus delayed crosstalk percentage as a function of the overvoltage.

requirements. For the DCR, which is a key parameter in the choice of the photodetectors for the DUNE FD, we can see that the values are included in the rage [50-80] mHz/mm^2 for the tested overvoltages. It is worth noting that these values include the burst effect that increase the overall dark counts and is correlated to to ionizing radiation that crosses the sensor [12]. Since DUNE FD will be underground and will exploit purified materials, we thus expect a reduction of the burst effect with respect to that measured in surface laboratories during the characterization, and consequently a decrease in the global DCR when the SiPMs will be operated in the FD. However, even with bursts, the measured values for the DCR are within DUNE requirements. The trend of the correlated noise is shown in figure 9c and 9d for afterpulse and crosstalk effects respectively. Also all these values are compliant with DUNE specifications.

4 PDE at cryogenic temperatures

The absolute PDE is a key performance parameter of SiPMs. PDE is commonly defined as the product of three factors: the SiPM's fill factor, the probability of avalanche triggering, and the silicon's quantum efficiency (QE). QE measures the likelihood of incident photons generating an

electron-hole pair within the sensor's sensitive volume and depends on photon wavelength. At low temperatures the wider energy band gap reduces the quantum efficiency. Furthemore, at approximatively 80-90K, carrier freeze-out effects may lead to a decrease in PDE [13]. In [14], a a slight decrease in PDE with decreasing temperature was observed for the CRYO-NUV-HD technology. Therefore, it is essential to directly measure the PDE at the temperature of operation (87K in case of liquid argon) for the DUNE customized FBK NUV-HD-cryo 3T production.
The measurement of the PDE involves characterizing the SiPM response under a calibrated light source. In addition, when determining the PDE, is crucial to account for the intrinsic SiPMs secondary counts arising from delayed correlated noise (after-pulses and delayed optical cross-talk).

4.1 Experimental Setup

The measurement detailed in this paper were conducted by using the setup called Vacuum Emission Reflectivity Absorbance (VERA) built at TRIUMF in Vancouver to characterize the response of SiPMs at cryogenic temperatures [15].
In this setup, the SiPM sample under test was mounted on a cold finger cooled by liquid nitrogen and regulated by a control system to maintain the temperature with an accuracy better than 1 K. The setup is consisting of a vacuum chamber coupled with a light source from a Resonance Lyman-Alpha DC Lamp and a VM200 Resonance monochromator. In order to measure the absolute incident light flux into the SiPM the light was directed toward a Photo-Diode (AXUV 100G). The AXUV 100G Photo-Diode was previously calibrated, at LAr temperature, against a NIST calibrated Photo-Diode (XUV-100C). The SiPM and the AXUV 100G photodiode are both placed on a movable arm which allows for remote x-y positioning. The incident light selected by monochromator is directed alternatively toward the SiPM under test and the Photo-Diode. In order to avoid geometric factors the light spot ($1.2mm$ diameter) in contained within the area of both sensors. Throughout the measurement, light stability was monitored by an Hamamatsu PMT (R8486) after reflection by a gold coated mirror. The VERA system has already been used to measure the PDE at cryogenic operating temperature in the context of the nEXO ([16],[17]) and DarkSide experiments. A layout of the hardware setup is shown in figure 10.

The SiPM PDE was measured both in photon-counting mode and current mode. In the first case, the SiPM signal was amplified by a dedicated two-stage amplifier and then acquired by a CAEN DT5730B Digitizer Module. The SiPM pulses in this case are individually reconstructed and counted in order to estimate the SiPM rate which will be compared with absolute photon flux measured by Photo-Diode. When measured in current mode, a Keysight B2985 low noise picoammeter[1] were used for both the SiPM and the Photo-Diode. To minimize the noise induced on the Photo-Diode by other sources, a shielded low noise triax cable (Keithley 7078-TRX-1) were used. A MIDAS-Labview based control system [18] served as system interface and provided slow control of the entire hardware system.

[1]RMS noise with open input of ~140 aA

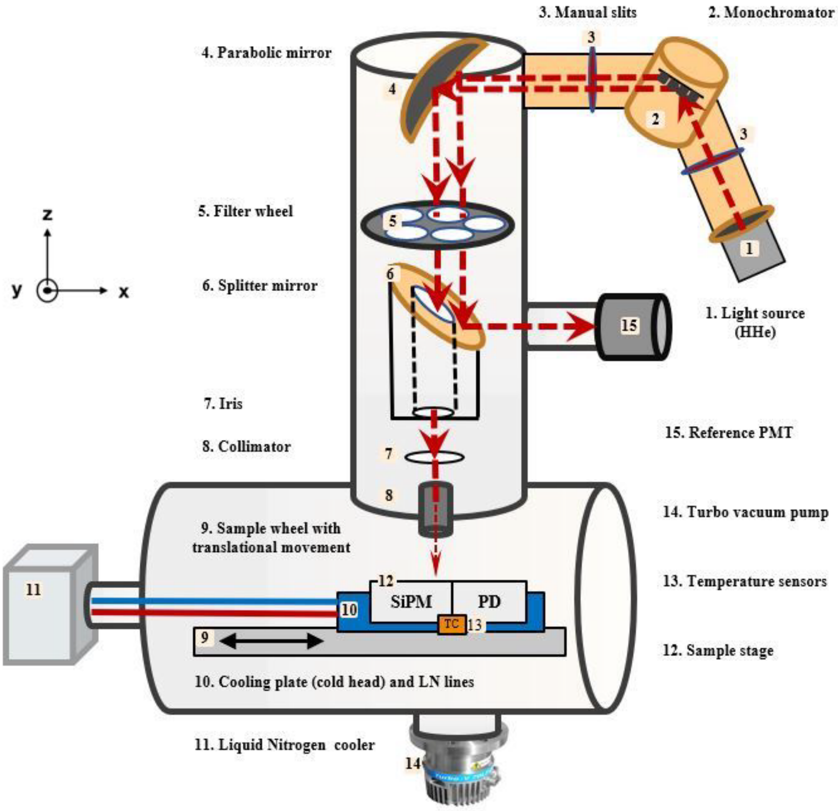

Figure 10. Hardware setup used for PDE measurement of FBK NUV-HD-cryo 3T sample at 87 K

4.2 PDE measurement procedure

The first step is to quantify the delayed correlated noise contribution of the SiPM under test as a function of the applied overvoltage. To achieve this, the light wavelength was set to 420 nm and light level was adjusted on a proper level to allow at same time for the pulse-counting of the individual waveforms and the S/N of the photodiode high enough to measure the light from DC lamp. Tipically, Photo-Diode currents of the order of $\sim$ 50 fA, were measured in these conditions. Since photons inducing avalanches and dark noise are uncorrelated events, they can be distinguished from correlated delayed avalanches by analyzing the time distribution of all pulse events relative to the primary pulse, as demonstrated in Ref. [19] . The total pulse rate, computed as function of the time difference, t, from the primary pulse ($t = 0$) is given by:

$$R(t) = R_{DC}(t) + R_{CDA}(t) + R_0(t) \tag{4.1}$$

where $R_{DC}(t)$ is the dark count rate, $R_{CDA}(t)$ is the rate of correlated delayed avalanches per pulse, and $R_0(t)$ is the rate of the photon induced avalanche detected by the SiPMs due to light source. In figure 11 the pulse rate R(t) measured at 87 K under 420 nm illumination, is shown as function of the time difference with respect to the primary pulse. As shown in [19] the rate of correlated delayed pulses is expected to vanish at sufficiently larger time. The primary pulse rate

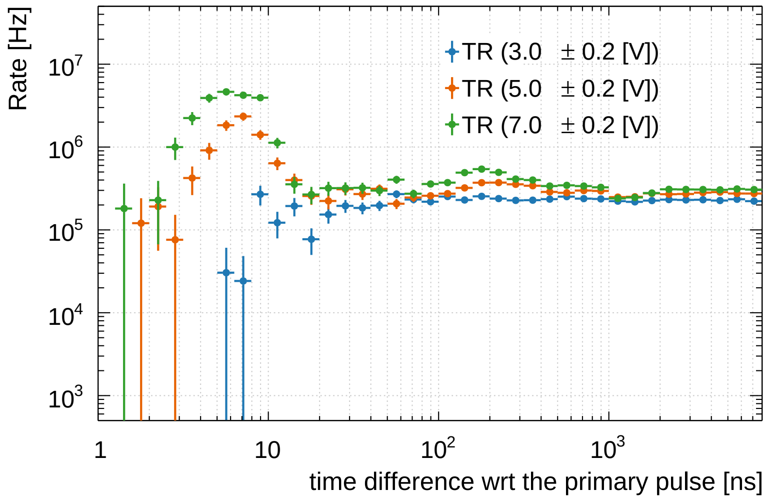

Figure 11. Observed pulse rate R(t) measured at 87K and 420 nm as a function of time differences with respect to the primary pulse for FBK NUV-HD-cryo 3T sample. The distribution is shown when SiPM is biased at 3, 5, 7 V overvoltages.

$R(t) = R_{DC}(t) + R_0(t)$, due to dark count and light source, can then be estimated from the figure 11, performing a weighted mean of the asymptotic rate at long times (t > 1 × 10^3 ns). Since R_{DC} is independently measured in the absence of light (with the Iris closed), by using the same method of the rate plot, the true photon-induced rate $R_0(t)$ can be measured. The SiPM PDE at 420 *nm* can be obtained dividing the measured SiPM primary count rate by the the photon flux Φ_0 measured by moving the calibrated photodiode under the light beam and defined as

$$\Phi_0 = \frac{(I - I_{DCR})\lambda}{R(\lambda)hc} \tag{4.2}$$

where I and I_{DCR} are the photodiode currents with and without illumination, respectively, R is the photodiode responsivity at the wavelength λ, h is Planck's constant and c is the speed of light. The PDE at 420 *nm* then is given by

$$PDE_{420} = \frac{R_0(t)}{\Phi_0} \tag{4.3}$$

By following this procedure, the quantity PDE_{420} has been measured as a function of the applied overvoltage from 3 V up to 8 V (Fig. 12).

Measuring the PDE in counting mode is too time-consuming to be performed at every wavelength. The PDE as function of wavelength values can be determined by measuring the currents of the photodiode and the SiPM for wavelengths scanned by monochromator. Specifically, the SiPM current at a given wavelength λ and applied overvoltage V is connected to the PDE through the following formula

$$I_{SIPM}(V,\lambda) - I^{DCR}_{SIPM}(V) = \Phi_0(\lambda) \times PDE(V,\lambda) \times f(V) \tag{4.4}$$

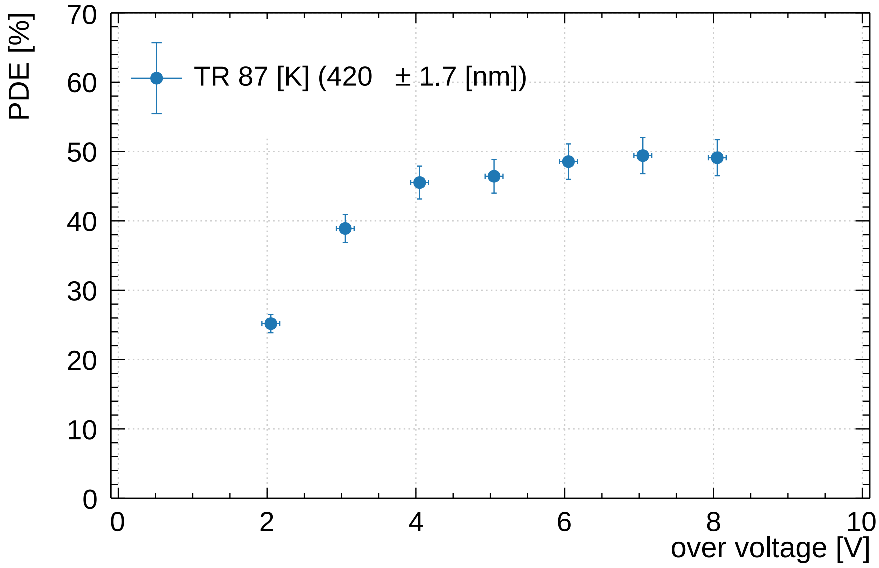

Figure 12. Photon Detection Efficiency measured at 420 nm and 87K as a function of the applied overvoltage for the FBK NUV-HD-cryo 3T sample.

where $I_{SIPM}(V,\lambda)$ and $I^{DCR}_{SIPM}(V)$ are the SiPM current with and without illumination at the wavelength λ, $\Phi_0(\lambda)$ is the photon flux rate measured with photodiode for light illumination at wavelenght λ, and $f(V)$ is a correction factor that accounts for the SiPM gain and for the correlated avalanche noise, which artifically increase the total SiPM output current. It can be written as

$$f(V) \sim q_e \times (1 + ECF) \times G \tag{4.5}$$

where ECF is the extra charge factor and G is the SiPM gain. It is possible to consider $f(V)$ as a function of the applied bias voltage and to be wavelength-independent because it depends only on the intrinsic characteristics of the SiPM.

In this work $f(V)$ is estimated at 87K by illuminating SiPMs with continous light source at 420 nm as follows:

$$f(V) = \frac{I_{SIPM}(V,420) - I^{DCR}_{SIPM}(V)}{\Phi_0(420) \times PDE(V,420)} \tag{4.6}$$

where we take advantage of the fact that the quantity $PDE(V,420)$ was previously measured in counting mode.

Once we extracted the wavelength independent factor $f(V)$ for each bias voltage it is possible to measure the PDE for a different wavelength as follows:

$$PDE(V,\lambda) = \frac{I_{SIPM}(V,\lambda) - I^{DCR}_{SIPM}(V)}{\Phi_0(\lambda) \times f(V)} \tag{4.7}$$

where $\Phi_0(\lambda)$ is defined in eq.4.2, $I_{SIPM}(V,\lambda)$ and $I^{DCR}_{SIPM}(V)$ are the SiPM current with and without the λ illumination. Figure 13 shows the PDE as a function of illumination wavelength, ranging

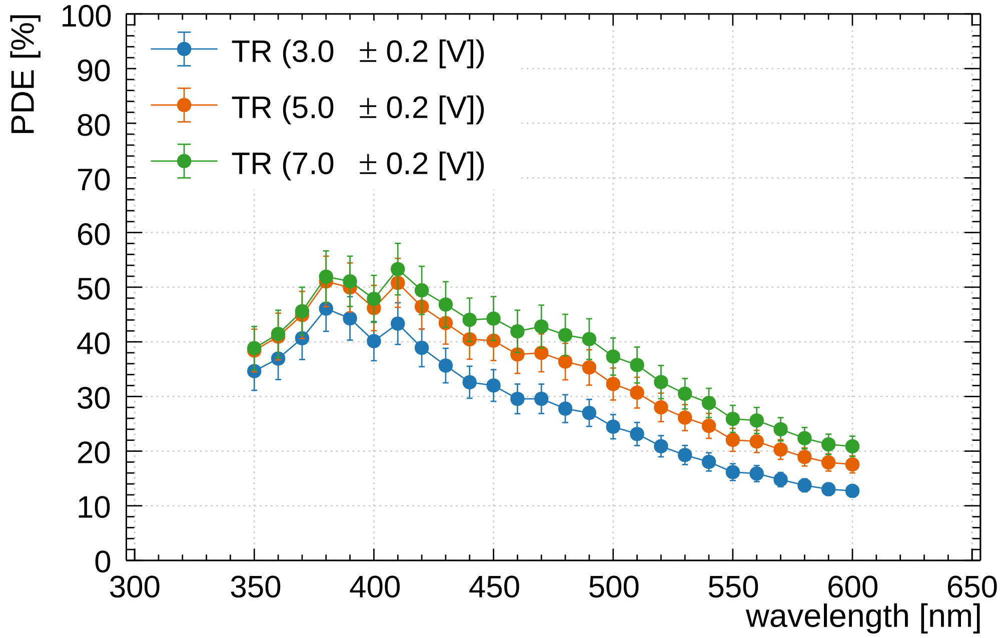

Figure 13. Photon Detection Efficiency measured at 87K as a function of the wavelength in the range 350-600 nm and of the applied overvoltages 3, 5 and 7 V for the FBK NUV-HD-cryo 3T sample.

from 350 nm to 600 nm in 10 nm increments, and SIPM overvoltage, varying for 3, 5 and 7 V. The error bars on each point includes statistical and systematic uncertainties.

The PDE measurement have been performed at 87 K temperature. The obtained results are in excellent agreement with the measurements performed at 90 K, as reported in [14]. We also report in figure 14 a comparison of the PDE measured at FBK Institute for the same device at room temperature (300 K) at wavelenght of 420 nm.

5 Conclusions

In this paper we described the characteristics and the measurements performed to the NUV-HD-cryo 3T SiPM from FBK in order to validate this sensor for the DUNE PDS. FBK sucesfully developed this sensor for DUNE with proprietary technologies aiming a high gain while keeping low the cross-talk probability. FBK together with the DUNE PDS consortium performed the validation tests of these sensors whose results are shown in this publication.

The FBK NUV-HD-cryo 3T sensor, together with HPK S13360-9935 were selected for the DUNE FD1-HD PDS. Comparing the FBK and the HPK sensors, both provide similar characteristics in terms of gain and correlated noise but the sensor from FBK requires a larger over-voltage for a similar PDE, nevertheless, as the breakdown voltage is lower than for the HPK sensors, the operation voltage (for the same PDE) is lower that the required by the HPK sensors.

During the DCR measurements, the appearance of pulse trains (bursts), as also happens with the HPK sensors, increases the DCR value expected at cryogenic temperatures but still meets the

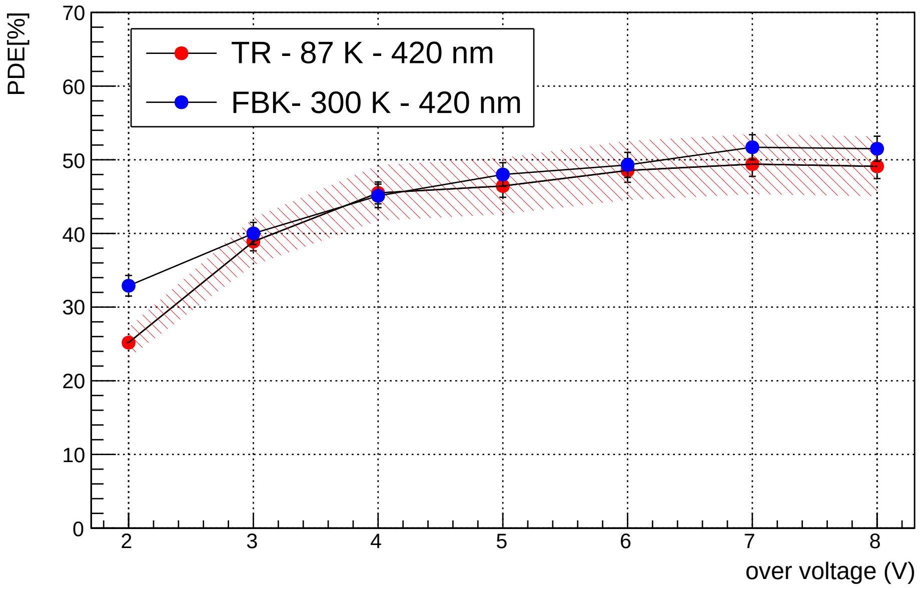

Figure 14. Photon Detection Efficiency measured at FBK for 420 nm and 300 K as a function of the overvoltage (blue dots) and the one measured at TRIUMF for 420 nm and 87 K (red dots) for the FBK NUV-HD-cryo 3T sample. The dashed area represents the region of systematic error in the measurement at 87 K.

DUNE requirements. Those requirements are not very strict because DCR will be dominated by the radiogenic background (39Ar) and achieving the lowest possible DCR is not a critical requirement. Still, a complete understanding of the origin of the DCR burst and the optimal layout of the array field may require further investigation, mainly for experiments with tighter radiogenic constraints.

We also presented a method and the results of the sensor PDE measurement in the wavelengths range from 350 nm to 600 nm at liquid argon temperature of 87K in order to validate its performance for the DUNE experiment. Within the measurement errors, no reduction with respect to room temperature PDE have been observed.

Acknowledgments

The present research has been supported and partially funded by the Italian Ministero dell'Università e della Ricerca (PRIN 2017KC8WMB and PRIN 20208XN9TZ), by the European Union's Horizon 2020 Research and Innovation programme under Grant Agreement No 101004761 (AIDAinnova), by the European Union-Next Generation EU by MCIN/AEI/10.13039/501100011033 under Grants no. PID2019-104676GB-C31, No. PID2019-104676GB-C32 & RYC2022-036471-I and PRE2020–094863 of Spain, and finally by the University of Ferrara (FIR2023), the BiCoQ Center of the University of Milano Bicocca and Leonardo Grant for Researchers in Physics 2023 BBVA Foundation.

We would like to thank the workshop staff from the INFN Ferrara section, namely Alessandro Saputi, Michele Cavallina and Stefano Squerzanti and from the INFN Milano Bicocca section,

namely Giancarlo Ceruti, Roberto Mazza, Roberto Gaigher.

References

[1] DUNE collaboration, *Deep Underground Neutrino Experiment (DUNE), Far Detector Technical Design Report, Volume I Introduction to DUNE*, *JINST* **15** (2020) T08008 [2002.02967].

[2] T. Heindl, T. Dandl, M. Hofmann, R. Krücken, L. Oberauer, W. Potzel et al., *The scintillation of liquid argon*, *Europhysics Letters* **91** (2010) 62002.

[3] H. Souza, E. Segreto, A. Machado, R. Sarmento, M. Bazetto, L. Paulucci et al., *Liquid argon characterization of the X-ARAPUCA with alpha particles, gamma rays and cosmic muons*, *JINST* **16** (2021) P11002.

[4] M. Andreotti, S. Bertolucci, A. Branca, C. Brizzolari, G. Brunetti, R. Calabrese et al., *Cryogenic characterization of hamamatsu hwb mppcs for the dune photon detection system*, *Journal of Instrumentation* **19** (2024) T01007.

[5] A. Gola, F. Acerbi, M. Capasso, M. Marcante, A. Mazzi, G. Paternoster et al., *Nuv-sensitive silicon photomultiplier technologies developed at fondazione bruno kessler*, *Sensors* **19** (2019) 308.

[6] C. Piemonte, A. Ferri, A. Gola, T. Pro, N. Serra, A. Tarolli et al., *Characterization of the first fbk high-density cell silicon photomultiplier technology*, *IEEE Transactions on Electron Devices* **60** (2013) 2567.

[7] F. Acerbi, G. Paternoster, A. Gola, N. Zorzi and C. Piemonte, *Silicon photomultipliers and single-photon avalanche diodes with enhanced nir detection efficiency at fbk*, *Nuclear Instruments and Methods in Physics Research Section A: Accelerators, Spectrometers, Detectors and Associated Equipment* **912** (2018) 309.

[8] F. Acerbi, S. Davini, A. Ferri, C. Galbiati, G. Giovanetti, A. Gola et al., *Cryogenic characterization of fbk hd near-uv sensitive sipms*, *IEEE Transactions on Electron Devices* **64** (2017) 521.

[9] C. Piemonte, A. Ferri, A. Gola, A. Picciotto, T. Pro, N. Serra et al., *Development of an automatic procedure for the characterization of silicon photomultipliers*, in *2012 IEEE Nuclear Science Symposium and Medical Imaging Conference Record (NSS/MIC)*, pp. 428–432, IEEE, 2012.

[10] G. Zappalà et al., "Set-up and methods for sipm photo-detection efficiency measurements, 2016."

[11] C. Brizzolari, P. Carniti, C. Cattadori, E. Cristaldo, A. de la Torre Rojo, M. Delgado et al., *Cryogenic front-end amplifier design for large sipm arrays in the dune fd1-hd photon detection system*, *Journal of Instrumentation* **17** (2022) P11017.

[12] M. Guarise, M. Andreotti, R. Calabrese, A.C. Ramusino, V. Cicero, M. Fiorini et al., *A newly observed phenomenon in the characterisation of sipm at cryogenic temperature*, *Journal of Instrumentation* **16** (2021) T10006.

[13] G. Collazuol, M.G. Bisogni, S. Marcatili, C. Piemonte and A. Del Guerra, *Studies of silicon photomultiplier at cryogenic temperatures*, *Nuclear Instruments and Methods in Physics Research Section A: Accelerators, Spectrometers, Detectors and Associated Equipment* **628** (2011) 389.

[14] F. Acerbi, G. Paternoster, S. Merzi, N. Zorzi and A. Gola, *NUV and VUV sensitive Silicon Photomultipliers technologies optimized for operation at cryogenic temperatures*, *Nuclear Instruments and Methods in Physics Research Section A: Accelerators, Spectrometers, Detectors and Associated Equipment* **1046** (2023) 167683.

[15] G. Gallina, *Development of a single vacuum ultra-violet photon-sensing solution for nEXO*, *PhD Thesis, The University of British Columbia (Vancouver)* (2021) .

[16] G. Gallina et al., *Characterization of the hamamatsu VUV4 MPPCs for nEXO*, *Nuclear Instruments and Methods in Physics Research Section A: Accelerators, Spectrometers, Detectors and Associated Equipment* **940** (2019) 371.

[17] G. Gallina et al., *Performance of novel VUV-sensitive Silicon Photo-M ultipliers for nEXO*, *The European Physical Journal C, Particle and Fields* **82** (2022) 12.

[18] MIDAS, *Maximum Integrated Data Acquisition System Development*, *https://midas.triumf.ca* .

[19] A. Butcher, L. Doria, J. Monroe, F. Retiere, B. Smith and J. Walding, *A method for characterizing after-pulsing and dark noise of PMTs and SiPMs*, *Nuclear Instruments and Methods in Physics Research Section A: Accelerators, Spectrometers, Detectors and Associated Equipment* **875** (2017) 87.